Article

Ultrasensitive Immunosensor for Cardiac Troponin I Detection Based on the Electrochemiluminescence of 2D Ru-MOF Nanosheets

Mengxia Yan, Jing Ye, Qiuju Zhu, Liping Zhu, Jianshe Huang, and Xiurong Yang

Anal. Chem., **Just Accepted Manuscript** • DOI: 10.1021/acs.analchem.9b02169 • Publication Date (Web): 25 Jun 2019

Ultrasensitive Immunosensor for Cardiac Troponin I Detection Based on the Electrochemiluminescence of 2D Ru-MOF Nanosheets

Mengxia Yan, †,‡ Jing Ye,‡ Qiuju Zhu,‡ Liping Zhu,‡ Jianshe Huang,*† Xiurong Yang*†§

†State Key Laboratory of Electroanalytical Chemistry, Changchun Institute of Applied Chemistry, Changchun, Jilin 130022, China

‡University of Science and Technology of China, Hefei, Anhui 230026, China

§University of Chinese Academy of Sciences, Beijing 100049, China

*Fax: +86 431 85689278. E-mail: xryang@ciac.ac.cn, huangjs@ciac.ac.cn

ABSTRACT: Electrochemiluminescence (ECL)-functionalized metal-organic frameworks (MOFs) have attracted increasing attention in biosensing in virtue of its diverse and tunable optical properties. A famous ECL luminophore, carboxyl-rich tris(4,4′-dicarboxylicacid-2,2′-bipyridyl) ruthenium(II) ($Ru(dcbpy)_3^{2+}$) possesses the characteristics of good water solubility and excellent ECL performance, which also has the potential to be organic ligand of metal-organic frameworks. Herein, functionalized MOF nanosheets (RuMOFNSs) containing plenty of $Ru(dcbpy)_3^{2+}$ in the frameworks was synthesized in aqueous solution by simple one-pot method. In this protocol, $Ru(dcbpy)_3^{2+}$ acted as organic ligand to coordinate with Zn^{2+} originated from $Zn(NO_3)_2$, polyvinylpyrrolidone (PVP) was used as structure-directing agent to control the formation of sheet-like structure. For the practical application, a "signal-on" ECL immunosensor was designed for cardiac troponin I (cTnI) detection by employing RuMOFNSs as ECL probe. The immunosensor exhibited high sensitivity and excellent selectivity for cTnI detection in the range from 1 fg/mL to 10 ng/mL with a detection limit as low as 0.48 fg/mL. Finally, the biosensor was successfully applied for the detection of cTnI in human serum sample with satisfactory results, demonstrating its potential application in bioanalysis and clinical diagnosis.

Electrochemiluminescence (ECL) as an analytical technique has attracted increasing attention in clinical diagnosis and environmental assays due to the controllability in temporal, space and light emitting intensity, simple operation, cost-effectiveness, high sensitivity, and low background signal.[1-4] Among various ECL emitters, tris (2,2′-bipyridyl)-ruthenium(II) ($Ru(bpy)_3^{2+}$) and its derivatives are most commonly employed luminophores owing to their regenerability.[5] In early stage, solution-phase $Ru(bpy)_3^{2+}$ ECL systems not only increased the waste of expensive reagents, but merely got limited luminous efficiency.[6,7] Nowadays, with the development of nanotechnology, researchers focused on immobilizing $Ru(bpy)_3^{2+}$ derivatives on the electrode surface with nanomaterials as carrier to overcome these shortcomings.[8,9] In general, $Ru(bpy)_3^{2+}$ derivatives exist in nanomaterials in two forms. One form is that $Ru(bpy)_3^{2+}$ derivatives as guest molecule are incorporated into nanomaterials by adsorption,[10] coordination effect,[11] cross-linking,[12] doping[13] or encapsulating.[14,15] For example, liposomes,[16] silica,[3] quantum dots,[5] noble metal nanomaterials[17] and 3D metal-organic frameworks[13] were used as carriers to load $Ru(bpy)_3^{2+}$ derivatives, which subsequently were utilized as ECL probes to design biosensors. Despite these methods improved the loading capacity and ECL efficiency of luminescent molecules, the immobilization process makes the synthesis of materials more tedious.[7] Additionally, the leakage of ECL luminophore is inevitable because they are just physically absorbed or entrapped into the nanomaterials.[3,11] In another form, $Ru(bpy)_3^{2+}$ derivatives were directly utilized as precursors to synthesize nanomaterials with various shapes.[18-21] For example, Chen et al. fabricated a hollow porous polymeric nanospheres (Ru-HPNSs) using polyethylenimine-ruthenium complex (PEI-Ru) as precursors and then used it as ECL probe to construct ultrasensitive aptasensor for mucin 1 detection.[18] $Ru(bpy)_3^{2+}$ nanowires with excellent ECL emission efficiency was synthesized by solvent evaporation induced self-assembly process with $Ru(bpy)_3(PF_6)_2$ as the only component.[19] This hollow porous or low dimensional nanostructure has a large specific, which could decrease inactive emission from tightly packed molecules in bulk materials.[18] Overall, nanomaterials directly prepared using $Ru(bpy)_3^{2+}$ derivatives as reactive components may improve the immobilized quantity of $Ru(bpy)_3^{2+}$ derivatives compared with the first method,[7] and can effectively prevent the luminophores from leaking. Therefore, it is desirable but a great challenge to prepare ECL nanomaterials with high stability, large specific surface area and high loading amount of $Ru(bpy)_3^{2+}$ derivatives.

Metal-organic frameworks (MOFs) were constructed by assembling organic ligands with metal ions/clusters via coordination reaction.[22-26] Benefiting from large surface area, chemical tunability and high loading capacity, MOFs had been applied to several fields including luminescence, gas storage and catalysis. Nowadays, some scientists had turned their attention to the ECL molecules functionalized MOFs and to design various ECL biosensors. However, most literatures just utilize the high loading capacity of MOFs to physically encapsulate ECL molecules,[11,13,27,28] a few works directly use ECL luminophore as organic ligand to synthesize Ru-MOFs.[29-31] Moreover, compared to the bulk MOF crystals, two-dimensional (2D) MOF nanosheets expose more accessible active sites on the large surface and promote the contact with substrate molecules, which furtherance the sensing performance of MOFs.[21,32-34] 2D MOF nanosheets can be directly obtained by using the structure-directing effect of PVP without post-synthetic exfoliation process.[33] For the synthesis of MOFs, the ligands

always possess some specific functional groups (-NH_2, -COOH, etc.). Inspired by this, $Ru(bpy)_3^{2+}$ derivative tris(4,4′-dicarboxylicacid-2,2′-bipyrid- yl) ruthenium (II) dichloride ($Ru(dcbpy)_3^{2+}$), a metal ligand containing six carboxyl groups in the symmetric position, can be used as ligand to synthesize Ru-MOF. [30,35,36] This synthetic method is a powerful strategy to fulfil the requirements of $Ru(bpy)_3^{2+}$ derivatives as host molecules. Subsequently, the synthesized Ru-MOF was expected to not only increase the load number but also prevent the leakage of ECL luminophore in the process of applications.

In this work, we synthesized a novel Ru-MOF nanosheets (RuMOFNSs) by a simple one-pot method based on the cooperative self-assembly reaction of Zn^{2+} and $Ru(dcbpy)_3^{2+}$ as organic ligands. $Ru(dcbpy)_3^{2+}$ are water-soluble, making it possible to synthesize MOFs in aqueous phase and avoiding environmental pollution caused by organic solvents. The highly exposed $Ru(dcbpy)_3^{2+}$ reactive sites, large surface area and abundant functionalized groups of the synthesized RuMOFNSs are expected to enhance ECL efficiency and to facilitate the loading of antibodies for immunoassay. Therefore, a cathode ECL immunosensor was proposed with the RuMOFNSs as signal probe for the determination of cTnI, an important biomarker of acute myocardial infarction (AMI).[37-39] Scheme 1 briefly summarized the preparation process of RuMOFNSs and the assembly process of immunosensor. This sensing platform exhibited excellent analytical performance for the detection of cTnI, which held great application prospect for target proteins detection in clinical analysis.

Scheme 1. Schematic Diagram for the Fabrication Process of ECL immunosensor

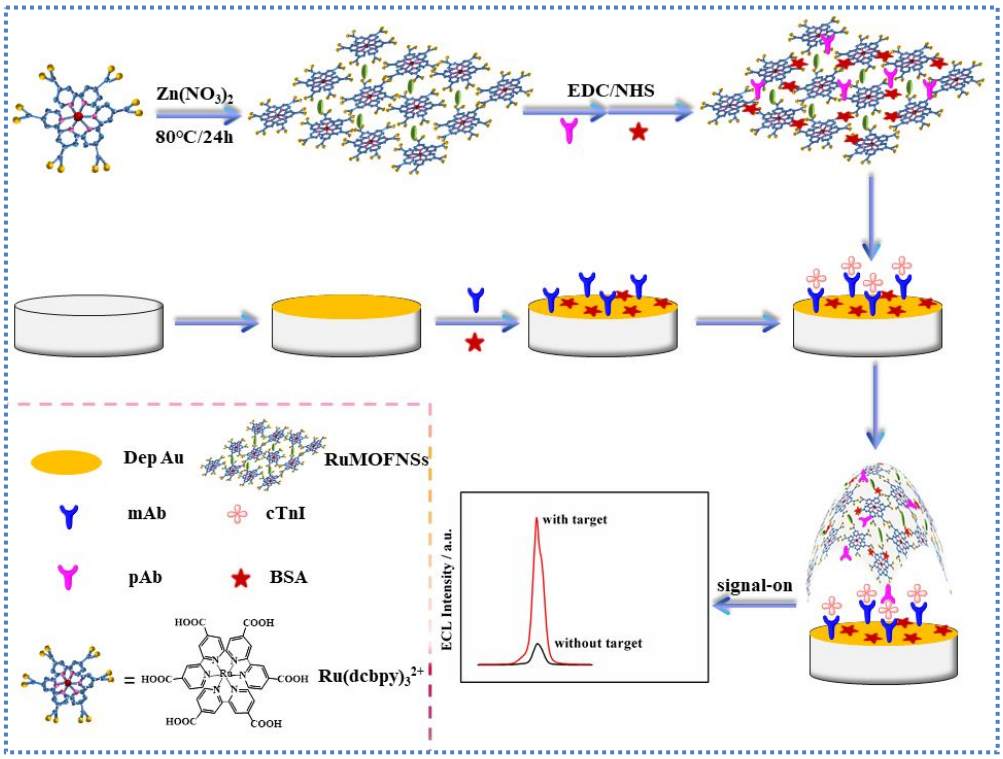

EXPERIMENTAL SECTION

Chemicals and Materials. Zinc nitrate hexahydrate ($Zn(NO_3)_2 \cdot 6H_2O$, 99%) was gained from J&K Scientific Ltd.(Beijing, China). 1-Ethyl-3-[3-(dimethylamino)-propyl] carbodiimide hydrochloride (EDC), N-hydroxysuccinimide (NHS), Polyvinylpyrrolidone (PVP, Mw=40,000), Pyrazine (99%) and albumin from bovine serum (BSA) were purchased from Sigma-Aldrich. Tris (4,4′-dicarboxylicacid-2,2′-bipyridyl) ruthenium(II) dicbloride ($Ru(dcbpy)_3^{2+}$) was acquired from Suna Tech Inc (Suzhou, China). Other reagents were bought from Beijing Chemical Reagent Company (Beijing, China). Phosphate buffer solution a (PBSa, pH 7.4, 0.1 M) and washing buffer solution (PBSb, pH 7.4, 0.01 M) were prepared using Na_2HPO_4 and NaH_2PO_4. The cardiac troponin (cTnI, cTnT and cTnC), anti-alpha fetoprotein (AFP) polyclonal antibody (rabbit, Ab_1), anti-cTnI monoclonal antibody (mouse, mAb) and polyclonal antibody (rabbit, pAb) were purchased form Abcam (Cambridge, MA). The human plasma was kindly supplied by the Second Hospital of Jilin University (Changchun, China). Unless otherwise specified, other reagents were of analytical grade and were used without further purification. Ultrapure water (18.2 MΩ cm) from a Millipore system was used in all aqueous solutions.

Apparatus. Transmission electron microscope (TEM), the scanning TEM (STEM) and the elemental mapping measurements of RuMOFNSs were acquired with a Tecnai G2 F20 S-TWIN electron microscope (FEI, American) and the accelerating voltage was 200 kV. Scanning electron microscope (SEM) images and energy dispersive X-ray spectroscopy (EDX) analysis were executed on a XL30 ESEM FEG microscope with an accelerating voltage of 20

kV. X-ray photoelectron spectroscopy (XPS) measurements were performed on an ESCALABMK II (VG Scientific) with Al Kα as the exciting source. X-ray powder diffraction (XRD) patterns were recorded with a D8-Advance system (Bruker, Germany) with Cu Kα radiation (λ=1.5406Å). UV-vis absorption characterization was performed on a CARY 50 Scan UV-vis spectrometer (Varian, USA). Atomic force microscopy (AFM) image was measured by Dimension Icon SPM (Bruker, Germany). FT-IR spectra were measured by Bruker VERTEX70 spectrometer (Ettlingen, Germany). ECL measurements were performed using MPI-E ECL analytical system (Xi'an Remex, China). The potential ranges from 0.00 to -1.60 V for cathodic scanning, with a scan rate of 100 mV/s, and photomultiplier tube (PMT) voltage of 450 V. The electrochemical and ECL measurements were performed with a three-electrode system, composing of Ag/AgCl reference electrode, platinum wire counter electrodes, and bare or modified glassy carbon electrode (GCE, d=3 mm) as working electrode. The electrolyte for ECL detection was PBSa solution (3 mL) containing 0.1 M KCl, and 0.1 M $K_2S_2O_8$ was added in the electrolyte as co-reactant.

Preparation of RuMOFNSs. $Zn(NO_3)_2{\cdot}6H_2O$ (9.0 mg), PVP (20 mg), $Ru(dcbpy)_3^{2+}$ (9.0 mg) and pyrazine (1.6 mg) were dissolved with 32 mL H_2O in a 50 mL round flask. After that, the solution was sonicated for 5 min to obtain a homogeneous solution. Then the flask was heated to 80 ℃ and kept for 24 h. The resulting orange crystals were centrifuged (12000 rpm, 10 min) and thoroughly washed three times with DI water. The obtained RuMOFNSs were eventually redispersed into water (0.24 mg/mL).

Modification of RuMOFNSs with Antibody. The as-prepared RuMOFNSs solution (1 mL, 0.24 mg/mL) was activated by 200 μL mixture solution of EDC/NHS (400 mM/100 mM) under the gently stirring at room temperature (RT) for 2 h, followed by adding 10 μL of pAb (1 mg/mL) and stirring overnight at 4 °C. Subsequently, the resulting RuMOFNSs-pAb bioconjugate was collected by centrifugal washing (12000 rpm, 10 min) with PBSb twice to remove free antibody. Finally, the RuMOFNSs-pAb was redispersed in 1 mL PBSb containing 1% BSA for 1 h to block the excess binding sites. After centrifugal washing, the resultant signal probe was dispersed with 1mL PBSb and stored at 4 ℃ for later use.

Fabrication of ECL immunosensor. The bare GCE was pretreated and electrodeposited a thin layer of Au NPs according to the reported literature.[40] Initially, the Au NPs modified GCE was incubated with 8 μL of mAb (10 μg/mL) for 12 h at 4 ℃ to absorb mAb onto the Au NPs layer. Thereafter, 4 μL of BSA (1%) solution was placed onto the electrode for 1h at RT to block the nonspecific adsorption sites. Next, the modified electrode mAb/Au NP/GCE was incubated with 10 μL of cTnI antigen (Ag) with a series of different concentrations and kept for 90 min, followed by further incubated with the RuMOFNSs-pAb bioconjugate for 1 h. The sandwiched type ECL immunosensor was fabricated by immunological recognition. After each modification step, the electrode was softly rinsed with 3-fold volume PBSb to remove weakly-bound components.

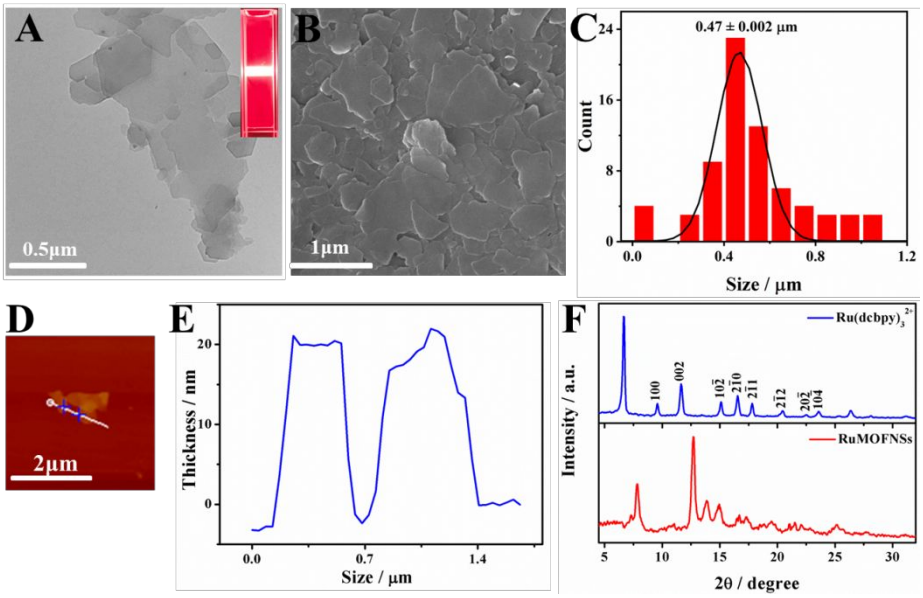

Figure 1. (A) TEM image and (B) SEM image of RuMOFNSs. The insert in (A) shows the Tyndall effect of RuMOFNSs (C) Statistical analyses of the lateral size of RuMOFNSs in SEM image. (D) AFM image of RuMOFNSs and (E) its section analysis. (F) XRD patterns of RuMOFNSs and $Ru(dcbpy)_3^{2+}$.

RESULTS AND DISCUSSION

Morphology characterization and element composition analysis of the as-synthesized RuMOFNSs. Simple one-pot synthesis of RuMOFNSs using $Ru(dcbpy)_3^{2+}$ (ECL luminophore) as organic ligand, pyrazine as crystallinity enhancing agent,[41] and PVP as structure-directing agent. The morphology of RuMOFNSs was characterized by TEM and

SEM, which showed obvious and irregular sheet-like structure with lateral size of 0.47±0.002 μm (Figure 1A–C). The Tyndall effect observed in the aqueous solution of RuMOFNSs indicated their colloidal structure (inset in Figure 2A). By using AFM and section analysis, the thickness of RuMOFNSs about 20 nm was measured (Figure 1D–E). As can be seen form Figure S1, the STEM image and the corresponding elemental mapping images indicated that uniform distribution of Ru and Zn elements in RuMOFNSs. The EDX spectrum further proved the existence of both Ru and Zn elements. The XRD characterization was performed to confirm the crystallinity of RuMOFNSs. The main diffraction peaks of RuMOFNSs were accorded with the reported literatures,[36,42] and significantly different from pure $Ru(dcbpy)_3^{2+}$ (Figure 1F).[19,28] Because the condition and solvent used in this work was different from others, some changes had taken place in the diffraction peak strength. These results confirmed that 2D MOF nanosheets were successfully synthesized with high crystallinity. XPS spectrum was also employed to explore the surface composition of RuMOFNSs. As shown in Figure 2A, XPS survey spectrum of RuMOFNSs shows the characteristic peaks of C 1s, N 1s, O 1s, Zn 2p, and Ru 3p. In particular, the high-resolution spectrum of Zn 2p shows two peaks centered at 1044.2 eV and 1021.1 eV, while the Ru 3p region displays the characteristic peaks of Ru $2p_{3/2}$ (462.1 eV) and Ru $2p_{1/2}$ (484.2 eV) (Figure 2B–C). The auger electron peak of Zn inserted into the Ru 3p region due to the simultaneous existence of Zn and Ru elements. The deconvoluted high-resolution XPS spectra of C 1s, N 1s and O 1s of RuMOFNSs are displayed in Figure S2. The IR spectrum of RuMOFNSs characterized peaks at 1721-1545 cm^{-1} and 1435-1370 cm^{-1} assigned to the symmetric and antisymmetric stretching vibration of the carboxylate ion (Figure 2D, curve a).[31,43,44] Similar to $Ru(dcbpy)_3^{2+}$ (Figure 2D, curve b), the bi-pyridine skeleton vibration located at 1609 cm^{-1} and 1545 cm^{-1}, and out-of-plane bending vibration peak of aromatic hydrogen bonds distributed in the range of 900-700 cm^{-1} demonstrated that Zn^{2+} replaced the hydrogen protons to form MOFs and the replacement didn't damage the structure of $Ru(dcbpy)_3^{2+}$.[43,45,46] All these results demonstrated the successfully synthesizing of RuMOFNSs.

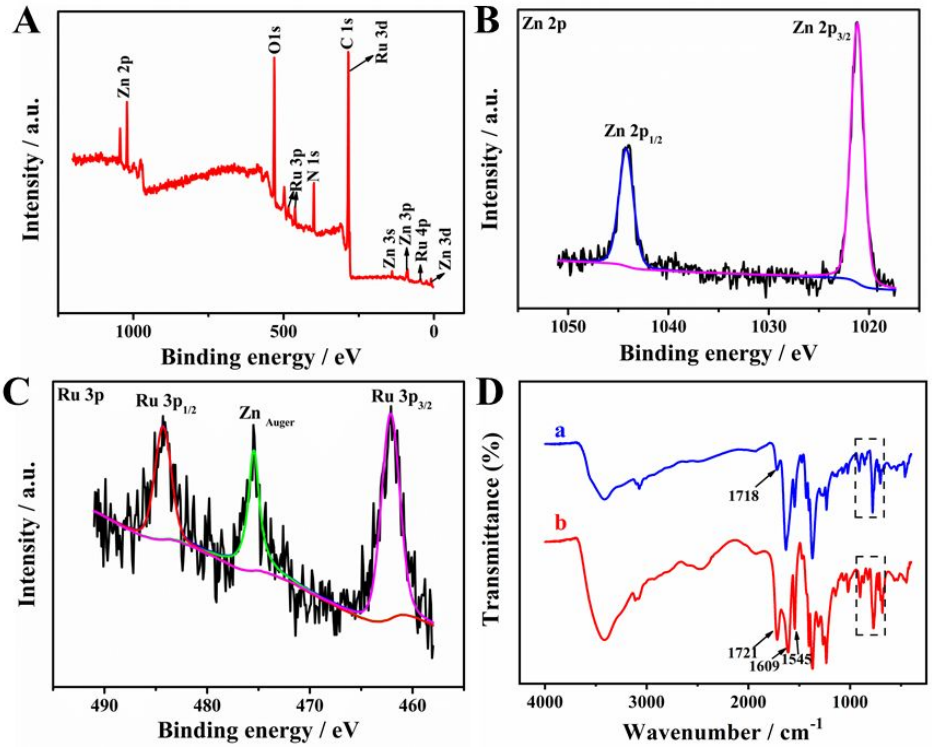

Figure 2. (A) XPS survey spectrum, the high-resolution (B) Zn 2p region, and (C) Ru 3p region of the synthesized RuMOFNSs. (D) FT-IR spectra of (a) RuMOFNSs and (b) $Ru(dcbpy)_3^{2+}$.

The photophysical properties of the RuMOFNSs. In the UV-vis absorption spectrum (Figure 3A, curve a), RuMOFNSs exhibite three peaks at 305 nm, 342-367 nm and 478 nm, which are related to the $\pi \rightarrow \pi^*$ electron transition of bi-pyridine ring, metal centred transition and the $d\pi(Ru) \rightarrow \pi^*(dcbpy)$ metal-to-ligand charge transfer (MLCT), respectively.[44,47] Compared with the free $Ru(dcbpy)_3^{2+}$ ligand (Figure 3A, curve b), the absorption peaks of RuMOFNSs have a slight red shift. These results stated the coordination interaction between carboxylic groups of $Ru(dcbpy)_3^{2+}$ and Zn^{2+}.[33] As shown in fluorescence spectra (Figure 3B), compared with the maximum exciting wavelength (λ_{ex}=489nm) and emission wavelength (λ_{em}=625 nm) of pure $Ru(dcbpy)_3^{2+}$, the corresponding wavelengths of RuMOFNSs shift to 498 and 638 nm, respectively. The red shift of the spectrum revealed some photons undergo energy transfer

and $Ru(dcbpy)_3^{2+}$ as the ligand distributed inside of the RuMOFNs.[30,44]

ECL mechanism of RuMOFNSs. The ECL spectrum was obtained by means of the optical filter technique for identify the ECL emitting species (Figure 4A, curve a). The ECL maximum emission wavelength of the RuMOFNSs at 635 nm was nearly identical with the fluorescence emission spectrum at 638 nm (curve b). In order to further clarify the reaction mechanism, synchronously cyclic voltammetry (CV) and ECL responses of different solutions were presented in Figure 4B. The CV curve of GCE in a RuMOFNSs solution showed a weak wave at -1.56 V (curve a), indicating that the $[RuMOFNSs]^+$ were produced by injection of an electron. For $S_2O_8^{2-}$ solution, an obvious reduction peak at -0.98V was ascribed to the electroreduction of $S_2O_8^{2-}$ (curve b).[48] Meanwhile very weak ECL signal was observed when the bare GCE was detected in RuMOFNSs or $K_2S_2O_8$ solution alone (curve a'-b'). The $K_2S_2O_8$ can be ECL emitter by using O_2 as co-reactant.[49] Due to the dissolved O_2 in the solution, the ECL intensity of $K_2S_2O_8$ is slightly higher than that of RuMOFNSs. Furthermore, in the mixture solution of RuMOFNSs and $K_2S_2O_8$, the electrode exhibited a reduction peak at -1.05 V with enhanced peak current. The negative shift of peak is caused by the increase of overpotential by the interaction between RuMOFNSs and $S_2O_8^{2-}$ (curve c).[13,50] At the same time, the corresponding ECL signal increased sharply (curve c'). All the conclusions indicated that RuMOFNSs is the ECL luminophore and $K_2S_2O_8$ as coreactant to promote the ECL efficiency. On the basis of above statement and previous literatures,[30,51,52] the possible cathodic ECL mechanism was presumed as follows, where $[RuMOFNSs]^{2+}$ represents the synthesized Ru-MOF nanosheets for more accurately depicting the mechanism. First, $S_2O_8^{2-}$ and $[RuMOFNSs]^{2+}$ was electrochemically reduced to $SO_4^{\bullet-}$ and $[RuMOFNSs]^+$ on the electrode surface (eq 1-2), Then, $SO_4^{\bullet-}$ as a strong oxidant can react with $[RuMOFNSs]^+$ to generate excited state $[RuMOFNSs]^{2+*}$ (eq 3). Finally, the unstable excited state releases energy back to the ground state in the form of light radiation (eq 4).

$$S_2O_8^{2-} + e^- \rightarrow SO_4^{2-} + SO_4^{\bullet-} \quad (1)$$

$$[RuMOFNSs]^{2+} + e^- \rightarrow [RuMOFNSs]^+ \quad (2)$$

$$[RuMOFNSs]^+ + SO_4^{\bullet-} \rightarrow [RuMOFNSs]^{2+*} + SO_4^{2-} \quad (3)$$

$$[RuMOFNSs]^{2+*} \rightarrow [RuMOFNSs]^{2+} + h\nu \quad (4)$$

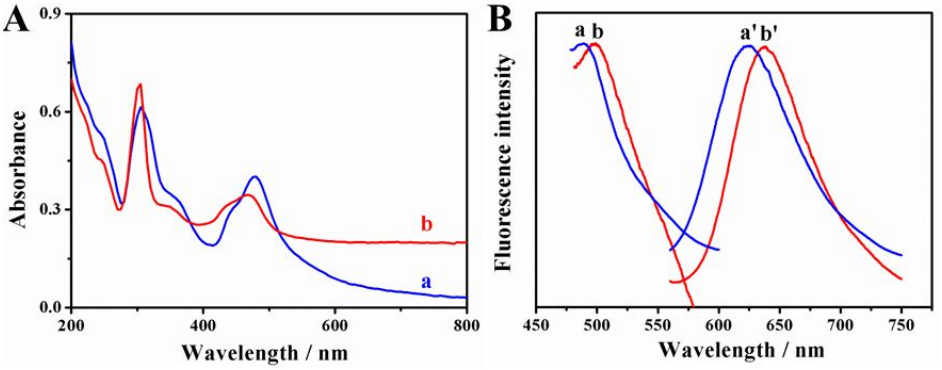

Figure 3. (A) UV-vis absorption spectra and (B) Fluorescence (FL) excitation and emission spectra of (a, a') $[Ru(dcbpy)_3]^{2+}$ and (b, b') RuMOFNSs.

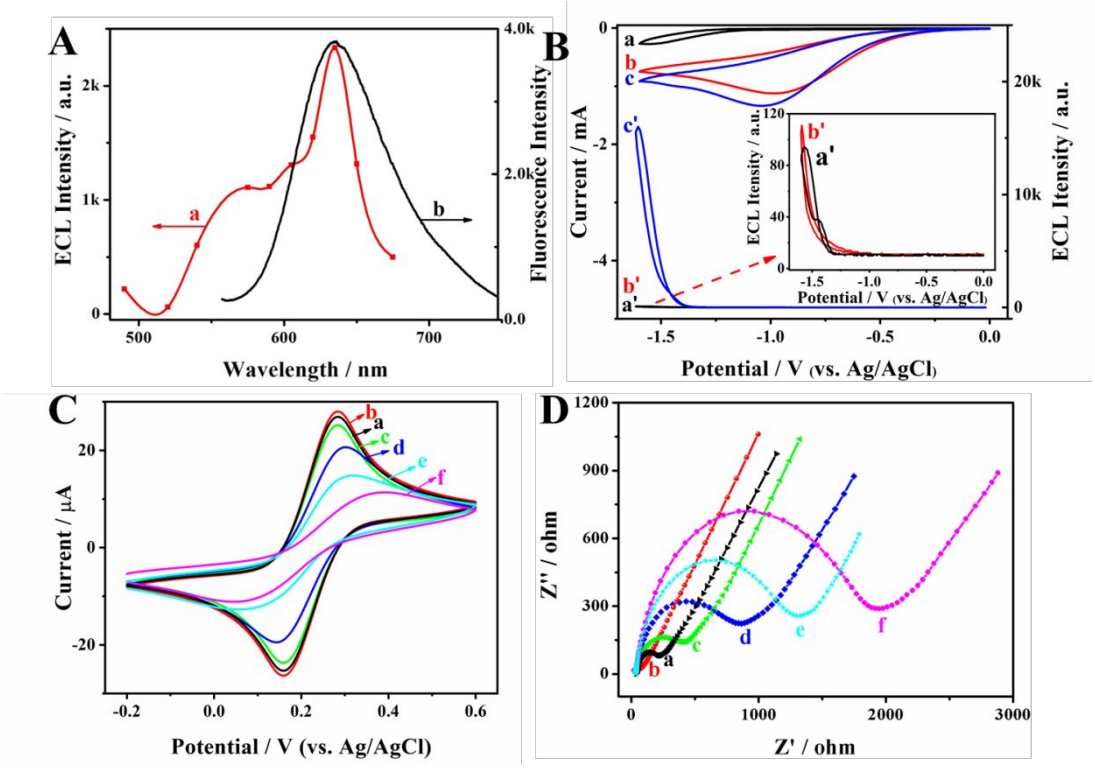

Figure 4. (A) ECL (a) and FL (b) (λ_{ex}=498 nm) spectra of RuMOFNSs. (B) CVs and ECL–potential plots of bare GCE in 5 mL PBS containing (a, a') RuMOFNSs (2.4 μg/mL), (b, b') $S_2O_8^{2-}$ (0.1 M), and (c, c') RuMOFNs (2.4 μg/mL) + $S_2O_8^{2-}$ (0.1 M), PMT =450 V. The insert shows the magnification of curve a' and b'. (C) CV and (D) EIS characterization of the stepwise modification of electrodes: (a) bare GCE, (b) depAu/GCE, (c) mAb/depAu/GCE, (d) BSA/mAb/depAu/GCE, and (e) cTnI/BSA/mAb/depAu/GCE, (f) RuMOFNSs-pAb/cTnI/BSA/mAb/depAu/GCE. The concentration of cTnI is 1 ng/mL.

Electrochemical behavior of the stepwise fabricated ECL immunosensors. Cyclic voltammetry and electrochemical impedance spectroscopy (EIS) are powerful techniques for monitoring the interface properties of the modified electrodes in the whole fabrication process.[53] CV and EIS experiments were performed in PBS (0.1 M, pH =7.4) containing 0.1 M KCl and 10.0 mM $[Fe(CN)_6]^{3-/4-}$ with scan rate of 50 mV/s. The bare GCE shows a couple of reversible redox peaks of $[Fe(CN)_6]^{3-/4-}$ (Figure 4C, curve a), while the redox peak currents increased evidently after the electro-deposition of Au NPs (depAu) on GCE, owing to the good conductivity and electron transfer promoting effect of Au NPs (Figure 4C, curve b). When mAb (capture probe) and BSA (blocking reagent) were grafted on the electrode surface via the stable Au-N bound between -NH_2 of proteins and depAu, the peak currents were successively decreased due to the poor conducting power of the proteins (Figure 4C, curve c, d). Finally, along with the modification of cTnI and the pAb/RuMOFNSs (signal probe) on electrode, the increased steric hindrance effect hindered electron transfer, accompanied by the further decrease of peak currents (Figure 4C, curve e-f). In the EIS measurements, a semi-circle represents the electron transfer-limited process and the diameter is equivalent to the electron transfer resistance (R_{et}), which reflects the electron transfer dynamics of the electrode. The bare GCE presents a small semicircle, while it is almost in a straight line after the deposition of gold nanoparticles, indicating the enhanced electron-transfer kinetics (Figure 4D, curve a–b). In the following steps, the electrode has been successfully modified according to the increasing R_{et} value (Figure 4D, curve c-f), caused by impeding of electron transfer by non-electroactive proteins. These results were consistent with CV, which proved the successful fabrication of the ECL immunosensor. Additionally, a control antibody of AFP (Ab_1) was used to substitute for pAb to prepare RuMOFNSs-Ab_1/cTnI/BSA/mAb/depAu/GCE. Compared with cTnI/BSA/mAb/depAu/GCE, the EIS spectrum of RuMOFNSs-Ab_1/cTnI/BSA/mAb/depAu/GCE showed the similar R_{et} value (Figure S4), indicating negligible RuMOFNSs-Ab_1 conjugate was immobilized on the electrode surface.

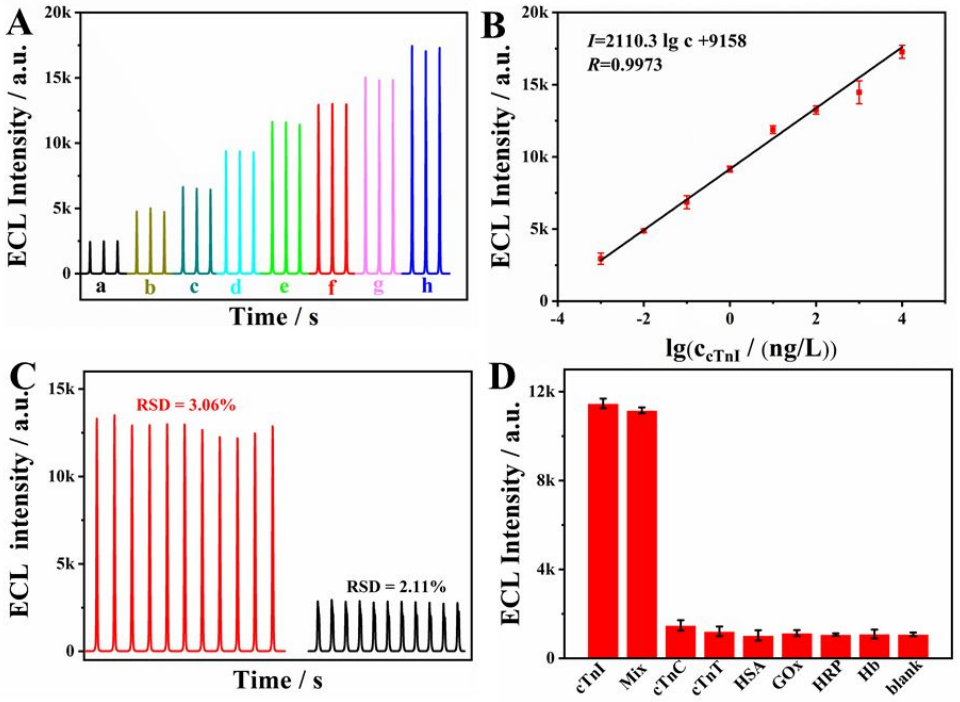

Figure 5. (A) ECL intensity-time curves and (B) the corresponding linear calibration plot of the ECL biosensor. The concentration of cTnI was: (a) 1 fg/mL, (b) 10 fg/mL, (c) 100 fg/mL, (d) 1 pg/mL, (e) 10 pg/mL, (f) 100 pg/mL, (g) 1 ng/mL and (h) 10 ng/mL. (C) Stability of the proposed ECL system incubated with 100 pg/mL (red line) or 1 fg/mL (black line) cTnI under 11 cycles of consecutive cyclic potential scanning. (D) Selectivity evaluation of the immunosensors with cTnI (10 pg/mL) and other non-target proteins (100 pg/mL).

Analytical performance of the ECL immunosensor in cTnI detection. The pH value, concentration of $K_2S_2O_8$, incubation time between mAb and cTnI were optimized for the sake of best sensing performance (Figure S3). Under the optimal conditions of pH=7.4, 0.1 M $K_2S_2O_8$ and 90 min of cTnI incubation time, the concentrations of cTnI were determined according to the proposed protocol. Within the range of 1 fg/mL-10 ng/mL, the ECL intensity versus the logarithmic values of target protein (cTnI) concentration showed well linear relationship (Figure 5A–B).The linear regression equation was I=2110.3 lg c + 9158 (unit of c is ng/L), and the correlation coefficient is 0.9973 (Figure 5B). The limit of detection (LOD) of the immunosensor was 0.48 fg/mL (S/N=3). Clinically, the concentration of cTnI from 0.5 to 2.0 ng/mL is regarded as the boundary between normal people and patients.[54] Thus this method can be used to detect cTnI in clinical samples. Compared with SERS, electrochemical, fluorescence and so on (Table S1), our method exhibits a wider linear detection range and higher sensitivity. The detection limit is comparable with the CdTe quantum dot-based ECL biosensor (0.46 fg/mL), but is significantly lower than those of other reported methods.[55]

Stability and selectivity of the ECL immunosensor. The operational stability of the ECL biosensor was evaluated by potential scanning of 11 consecutive cycles with 100 pg/mL and 1 fg/mL cTnI (Figure 5C). The relative standard deviations (RSDs) were 3.06% and 2.11%, respectively, indicating well stability of the designed ECL system. The selectivity of the proposed immunosensor was evaluated by ECL intensity toward blank and several interfering proteins including cTnC, cTnT, HSA, GOx, HRP and Hb. As can be seen from Figure 5D, cTnI and the mixture of cTnI and other proteins demonstrated similar ECL intensity, and the ECL responses of non-specific proteins were almost the same as the blank solution. These results solidly confirmed the designed ECL immunosensor had excellent specificity for cTnI detection. As shown in Figure S5, six immunosensors were prepared to detect 1 ng/mL cTnI. The RSD of ECL response is 2.56%, demonstrating the excellent fabrication reproducibility.

Analysis of cTnI in human serum sample. The practical application of the immunosensor was evaluated in human serum sample by using the standard addition method. The standard cTnI solution with different concentration was spiked to 20-fold diluted human serum, and then detected by the developed immunosensor. As listed in Table S2, the recovery of cTnI detection was in the range of 95.14%-104.75% and the RSD varied from 1.44% to 3.11%, illustrating that the designed immunosensor has favorable application prospects in cTnI detection and even clinical real samples analysis.

CONCLUSION

In this work, we synthesized a novel 2D MOF nanosheets with excellent ECL property by simple one-pot method with $Ru(dcbpy)_3^{2+}$ as organic ligand. The unique structure, and the abundant active sites and functional groups make this material as an ideal ECL probe. Benefiting from the ECL behavior of RuMOFNSs, a “signal-on” immunosensor was

constructed for the detection of cTnI. The immunosensor exhibited high sensitivity with a low limit of detection (0.48 fg/mL, S/N=3) and a wide linear range (1 fg/mL-10 ng/mL). Moreover, this immunosensor also showed good stability and selectivity for cTnI detection. In general, this work opens the way to prepare efficient ECL nanomaterials, and the as-synthesized materials can find broad applications in biological analysis and clinical diagnosis.

ASSOCIATED CONTENT

Supporting Information

The Supporting Information is available free of charge on the ACS Publications website.

STEM image, EDX elemental mapping images and EDX spectrum of RuMOFNSs (Figure S1), deconvoluted high−resolution XPS spectra of C 1s, O 1s and N 1s of RuMOFNSs (Figure S2), optimization of the reaction conditions (Figure S3), the selectivity evaluation of the immunosensors evaluated by EIS characterization (Figure S4), the fabrication reproducibility of the immunosensor (Figure S5), comparison of analytical performance of the developed ECL immunosensor with the reported methods (Table S1) and practical application of the proposed strategy (Table S2) (PDF)

AUTHOR INFORMATION

Corresponding Author

* E-mail: xryang@ciac.ac.cn. Phone: +86 431 85262056. Fax: +86 431 85689278.

* E-mail: huangjs@ciac.ac.cn Phone: +86 43185262964. Fax: +86 431 85689278.

Author Contributions

The manuscript was written through contributions of all authors.

Notes

The authors declare no competing financial interest.

ACKNOWLEDGMENT

This work was supported by the National Key Research and Development Program of China (2016YFA0201301), the National Natural Science Foundation of China (No. 21435005 and 21627808), the Key Research Program of Frontier Sciences, CAS (no. QYZDY-SSW-SLH019, and the Development Project of Science and Technology of Jilin Province (No. 20170101195JC).

REFERENCES

(1) Dang, J.; Guo, Z. H.; Zheng, X. W. *Anal. Chem.* **2014**, 86, 8943-8950.

(2) Liu, S. S.; Yuan, H. X.; Bai, H. T.; Zhang, P. B.; Lv, F. T.; Liu, L. B.; Dai, Z. H.; Bao, J. C.; Wang, S. *J. Am. Chem. Soc*. **2018**, 140, 2284-2291.

(3) Liang, W. B.; Zhuo, Y.; Xiong, C. Y.; Zheng, Y. N.; Chai, Y. Q.; Yuan, R. *Anal. Chem*. **2015**, 87, 12363-12371.

(4) Carrara, S.; Aliprandi, A.; Hogan, C. F.; De Cola, L. *J. Am. Chem. Soc*. **2017**, 139, 14605-14610.

(5) Carrara, S.; Arcudi, F.; Prato, M.; De Cola, L. *Angew. Chem., Int. Ed*. **2017**, 56, 4757-4761.

(6) Du, F. K.; Zhang, H.; Tan, X. C.; Yan, J.; Liu, M.; Chen, X.; Wu, Y. Y.; Feng, D. F.; Chen, Q. Y.; Cen, J. M.; Liu, S. G.; Qiu, Y. Q.; Han, H. Y. *Biosens. Bioelectron.* **2018**, 106, 50-56.

(7) Wang, H. J ; Yuan, Y. L.; Zhuo, Y.; Chai, Y. Q.; Yuan, R. *Anal. Chem*. **2016**, 88, 2258-2265.

(8) Valenti, G.; Rampazzo, E.; Bonacchi, S.; Petrizza, L.; Marcaccio, M.; Montalti, M.; Prodi, L.; Paolucci, F. *J. Am. Chem. Soc*. **2016**, 138, 15935-15942.

(9) Wang, H. J.; Yuan, Y. L.; Chai, Y. Q.; Yuan, R. *Small* **2015**, 11, 3703-3709.

(10) Zhang, L. H.; Xu, Z. A.; Sun, X. P.; Dong, S. J. *Biosens. Bioelectron.* **2007**, 22, 1097-1100.

(11) Hu, G. B.; Xiong, C. Y.; Liang, W. B.; Zeng, X. S.; Xu, H. L.; Yang, Y.; Yao, L. Y.; Yuan, R.; Xiao, D. R. *ACS Appl. Mater. Interfaces* **2018**, 10, 15913−15919

(12) Li, Z. Y.; Lin, Z. F.; Wu, X. Y.; Chen, H. T.; Chai, Y. Q.; Yuan, R. *Anal. Chem.* **2017**, 89, 6029-6035.

(13) Xiong, C. Y.; Liang, W. B.; Zheng, Y. N.; Zhuo, Y.; Chai, Y. Q.; Yuan, R. *Anal. Chem.* **2017**, 89, 3222-3227.

(14) Dong, X.; Zhao, G. H.; Liu, L.; Li, X.; Wei, Q.; Cao, W. *Biosens. Bioelectron.* **2018**, 110, 201-206.

(15) Li, X. J.; Yu, S. Q.; Yan, T.; Zhang, Y.; Du, B.; Wu, D.; Wei, Q. *Biosens. Bioelectron.* **2017**, 89, 1020-1025.

(16) Qi, H. L.; Qiu, X. Y.; Xie, D. P.; Ling, C.; Gao, Q.; Zhang, C. X. *Anal. Chem.* **2013**, 85, 3886-3894.

(17) Wang, H. J.; Chai, Y. Q.; Li, H.; Yuan, R. *Biosens. Bioelectron.* **2018**, 100, 35-40.

(18) Chen, A. Y.; Zhao, M.; Zhuo, Y.; Chai, Y. Q.; Yuan, R. *Anal. Chem.* **2017**, 89, 9232-9238.

(19) Li, Q.; Zheng, J. Y.; Yan, Y. L.; Zhao, Y. S.; Yao, J. N. *Adv. Mater.* **2012**, 24, 4745-4749.

(20) Xu, Y.; Yin, X. B.; He, X. W.; Zhang, Y. K. *Biosens. Bioelectron.* **2015**, 68, 197-203.

(21) Shao, H. L.; Lu, J.; Zhang, Q. Q.; Hu, Y. F.; Wang, S.; Guo, Z. Y. *Sens. Actuators, B.* **2018**, 268, 39-46.

(22) Kahn, J. S.; Freage, L.; Enkin, N.; Garcia, M. A.; Willner, I. *Adv. Mater.* **2017**, 29,1602782.

(23) Zhao, M. T.; Deng, K.; He, L. C.; Liu, Y.; Li, G. D.; Zhao, H. J.; Tang, Z. Y. *J. Am. Chem. Soc.* **2014**, 136, 1738-1741.

(24) Xu, G.; Yamada, T.; Otsubo, K.; Sakaida, S.; Kitagawa, H. *J. Am. Chem. Soc.* **2012**, 134, 16524-16527.

(25) Jiang, H. L.; Feng, D. W.; Wang, K. C.; Gu, Z. Y.; Wei, Z. W.; Chen, Y. P.; Zhou, H. C. *J. Am. Chem. Soc.* **2013**, 135, 13934-13938.

(26) Yang, C. X.; Yan, X. P. *Chin. J. Anal. Chem.* **2013**, 41, 1297-1300.

(27) Chen, R.; Zhang, J. F.; Chelora, J.; Xiong, Y.; Kershaw, S. V.; Li, K. F.; Lo, P. K.; Cheah, K. W.; Rogach, A. L.; Zapien, J. A.; Lee, C. S. *ACS Appl. Mater. Interfaces*. **2017**, 9, 5699-5708.

(28) Yin, H. Q.; Yang, J. C.; Yin, X. B. *Anal. Chem.* **2017**, 89, 13434-13440.

(29) Kent, C. A.; Liu, D. M.; Meyer, T. J.; Lin, W. B. *J. Am. Chem. Soc.* **2012**, 134, 3991-3994.

(30) Zhang, S. Q.; Han, L.; Li, L. N.; Cheng, J.; Yuan, D. Q.; Luo, J. H. *Cryst. Growth. Des.* **2013**, 13, 5466-5472.

(31) Zhu, S.; Lin, X.; Ran, P. Y.; Xia, Q.; Yang, C. C.; Ma, J.; Fu, Y. Z. *Biosens. Bioelectron.* **2017**, 91, 436-440.

(32) Huang, Y.; Zhao, M. T.; Han, S. K.; Lai, Z. C.; Yang, J.; Tan, C. L.; Ma, Q. L.; Lu, Q. P.; Chen, J. Z.; Zhang, X.; Zhang, Z. C.; Li, B.; Chen, B.; Zong, Y.; Zhang, H. *Adv. Mater.* **2017**, 29, 1700102.

(33) Zhao, M. T.; Wang, Y. X.; Ma, Q. L.; Huang, Y.; Zhang, X.; Ping, J. F.; Zhang, Z. C.; Lu, Q. P.; Yu, Y. F.; Xu, H.; Zhao, Y. L.; Zhang, H. *Adv. Mater.* **2015**, 27, 7372-7378.

(34) Shao, H. L.; Lin, H.; Lu, J.; Hu, Y. F.; Wang, S.; Huang, Y. J.; Guo, Z. Y. *Biosens. Bioelectron.* **2018**, 118, 247-252.

(35) Eddaoudi, M.; Kim, J.; Rosi, N.; Vodak, D.; Wachter1, J.; O'Keeffe, M.; Yaghi, O. M.. *Science* **2002**, 295, 469.

(36) Kent, C. A.; Mehl, B. P.; Ma, L. Q.; Papanikolas, J. M.; Meyer, T. J.; Lin, W. B. *J. Am. Chem. Soc.* **2010**, 132, 12767-12769.

(37) Jo, H.; Gu, H.; Jeon, W.; Youn, H.; Her, J.; Kim, S. K.; Lee, J.; Shin, J. H.; Ban, C. *Anal. Chem.* **2015**, 87, 9869-9875.

(38) Lou, D. D.; Fan, L.; Cui, Y.; Zhu, Y. F.; Gu, N.; Zhang, Y. *Anal. Chem.* **2018**, 90, 6502-6508.

(39) Ye, J.; Zhu, L. P.; Yan, M. X.; Zhu, Q. J.; Lu, Q. Q.; Huang, J. S.; Cui, H.; Yang, X. R. *Anal. Chem.* **2019**, 91, 1524−1531.

(40) Xie, S. B.; Dong, Y. W.; Yuan, Y. L.; Chai, Y. Q.; Yuan, R.

Anal. Chem. **2016**, 88, 5218-5224.
(41) Zhang, H,; Zhao, M. T. *U.S. Patent* 15 /762,328, **2017**.
(42) Zhang, S. Q.; Li, L. N.; Zhao, S. G.; Sun, Z. H.; Hong, M. C.; Luo, J. H. *J. Mater. Chem. A.* **2015**, 3, 15764-15768.
(43) Zhao, Y. W.; Jiang, L.;Li, S. H.; Li, M.; Liu, A. R.; Liu, S. Q. *J. Mater. Chem. A.* **2018,** 6, 2828-2833.
(44) Xiao, F. N.; Wang, M.; Wang, F. B.; Xia, X. H. *Small* **2014**, 10, 706-716.
(45) Qin, X. L.; Gu, C. Y.; Wang, M. H.; Dong, Y. F.; Nie, X.; Li, M. X.; Zhu, Z. W.; Yang, D.; Shao, Y. H. *Anal. Chem.* **2018**, 90, 2826−2832.
(46) Cui, L.; Wu, J.; Li, J.; Ju, H. X. *Anal. Chem.* **2015**, 87, 10635-10641.
(47) Shi, L.; Li, X. J.; Zhu, W. J.; Wang, Y. G.; Du, B.; Cao, W.; Wei, Q.; Pang, X. H. *ACS Sens.* **2017**, 2, 1774-1778.
(48) Lei, Y. M.; Wen, R. X.; Zhou, J.; Chai, Y. Q.; Yuan, R.; Zhuo, Y. *Anal. Chem.* **2018**, 90, 6851-6858.
(49) Lei, Y. M.; Huang, W. X.; Zhao, M.; Chai, Y. Q.; Yuan, R.; Zhuo, Y. *Anal. Chem.* **2015**, 87, 7787-7794.
(50) Ma, M.. N.; Zhuo, Y.; Yuan, R.; Chai, Y. Q. *Anal.Chem.* **2015**, 87, 11389-11397.
(51) Wang, Y. G.; Zhao, G. H.; Li, X. J.; Liu, L.; Cao, W.; Wei, Q. *Biosens. Bioelectron.* **2018**, 101, 290-296.
(52) Irkham; Watanabe, T.; Fiorani, A.; Valenti, G.; Paolucci, F.; Einaga, Y. *J. Am. Chem. Soc.* **2016**, 138, 15636-15641.
(53) Wang, L.; Liu, D. Q.; Sun, Y. L.; Su, J. J.; Jin, B. W.; Geng, L.; Song, Y. Y.; Huang, X.; Yang, M. *Anal. Chem.* **2018**, 90, 10858-10864.
(54) Han, X.; Li, S. H.; Peng, Z. L.; Othman, A. M.; Leblanc, R. *ACS Sens.* **2016**, 1, 106-114.
(55) Yang, X.; Yu, Y. Q.; Peng, L. Z.; Lei, Y. M.; Chai, Y. Q.; Yuan, R.; Zhuo, Y. *Anal. Chem.* **2018**, 90, 3995-4002.

For TOC only